Numerical Investigation of Effects of Rectangular Structure on Cavitation Evolution Around NACA0015 Hydrofoil

Yanyan Wang[1], Weiguo Zhao[1(✉)], Chao Wang[2], Xiangdong Han[3(✉)], Pengjun Fan[4], and Zailun Liu[1]

[1] College of Energy and Power Engineering, Lanzhou University of Technology, Lanzhou 730050, China
zhaowg@zju.edu.cn
[2] Chongqing Pump Industry Co., Ltd., Chongqing 400033, China
[3] School of Civil Engineering, Nanchang Institute of Technology, Nanchang 330044, China
fluidhanxd@126.com
[4] Machine Industry Lanzhou Petrochemical Equipment Inspection Institute Co., Ltd., Lanzhou 730070, China

Abstract. A combination of an improved SST k-ω turbulence model with Zwart-Gerber-Belamri cavitation model was employed to perform the numerical simulation of cavitation flow around general NACA0015 hydrofoil and the hydrofoil with rectangular structure on the surface. Effects of the rectangular structure on cavitation evolution were determined. Cavitation bubble evolution process and distribution of streamlines were investigated. Results clearly indicated that average lift-drag ratio of the hydrofoil with rectangular structure on the surface increased by 15.98%. Cavitation bubbles decreased and the distribution scopes of vortices reduced significantly. Cavitation evolution was effectively suppressed.

Keywords: Cavitation · Rectangular structure · NACA0015 hydrofoil · Numerical simulation

1 Introduction

Cavitation is one severe hydrodynamic problem, which significantly restricts the efficient and stable operation of hydraulic equipment, such as centrifugal pump [1]. Cavitation evolution process is closely associated with many diverse influence factors; the essence is phase change between liquid and vapor [2].

Cavitation bubble periodic evolution process could induce vibration and noise to let hydraulic machinery suffer serious destructions [3]. Therefore, investigations to retard cavitation onset and inhibit cavitation bubble shedding have received particularly extensive attentions [4]. Kawanami et al. [5] put the obstacle at the position of 37% chord length to leading edge of the hydrofoil to inhibit the re-entrant jet, which changed cavitation evolution process and the drag was significantly reduced. Jin [6] proposed one method that one single lateral wing was fixed at NACA0015 hydrofoil tail to suppress

L. Yan and J. Na (Eds.): ICFPMCE 2022, AHE 10, pp. 291–303, 2023.
https://doi.org/10.2991/978-94-6463-022-0_26

the separation of boundary layer flow; aim to control cavitation flow around NACA0015 hydrofoil was achieved. Zhang et al. [7] placed the obstacle on the flat hydrofoil surface to control cavitation bubble shedding. They found that under the action of the obstacle, cavitation bubble length had significant reduction; on the other hand, bubble shedding pattern changed from the large scale to the small scale. Liu et al. [8] slotted on Clark-Y hydrofoil to suppress the instability caused by cavitation; they got that jet formed at the slot exit interfered the re-entrant jet motion, which let cavitation bubble periodic shedding process was suppressed. Shi et al. [9] placed micro channel over the NACA0012 hydrofoil to connect internal low-pressure region to the external. Their results showed that the scale of cavitation reduced by 50%; cavitation generation and development were inhibited effectively.

In this paper, one rectangular structure with the size of 5.5 mm × 4 mm × 1.7 mm was put at the position of 55% chord length of NACA0015 hydrofoil suction surface. A comparative study of cavitation bubble shedding process and streamline distribution around general NACA0015 hydrofoil and the hydrofoil with rectangular structure was performed.

2 Mathematical Model

2.1 Fundamental Equation

For our numerical simulation, homogeneous mixture model was employed for the numerical simulation of cavitation flow around the hydrofoil. The primary and secondary phases are liquid and vapor, respectively. All fundamental equations [10] are shown as follows.

$$\frac{\partial \rho_{\mathrm{m}}}{\partial t} + \frac{\partial \left(\rho_{\mathrm{m}} u_j\right)}{\partial x_j} = 0 \tag{1}$$

$$\frac{\partial (\rho_{\mathrm{m}} u_i)}{\partial t} + \frac{\partial \left(\rho_{\mathrm{m}} u_i u_j\right)}{\partial x_j} = -\frac{\partial p}{\partial x_i} + \frac{\partial}{\partial x_j}\left(\mu_{\mathrm{m}} \frac{\partial u_i}{\partial x_j}\right) \tag{2}$$

$$\frac{\partial (\rho_{\mathrm{l}} \alpha_{\mathrm{l}})}{\partial t} + \frac{\partial \left(\rho_{\mathrm{l}} \alpha_{\mathrm{l}} u_j\right)}{\partial x_j} = m_{\mathrm{e}} - m_{\mathrm{c}} \tag{3}$$

where ρ_{m} is mixture density. μ_{m} is mixture viscosity. m_{e} and m_{c} are denoted as evaporation source term and condensation source term. u is mixture velocity. x indicates spatial coordinate. i and j are subscripts with values of 1, 2, and 3, respectively. ρ_{l} is the density of water and α_{l} is the corresponding volume fraction. p is pressure and t is time.

ρ_{m} and μ_{m} are defined below:

$$\rho_{\mathrm{m}} = \rho_{\mathrm{l}} \alpha_{\mathrm{l}} + \rho_{\mathrm{v}} \alpha_{\mathrm{v}} \tag{4}$$

$$\mu_{\mathrm{m}} = \mu_{\mathrm{l}} \alpha_{\mathrm{l}} + \mu_{\mathrm{v}} \alpha_{\mathrm{v}} \tag{5}$$

where ρ_{v} is the density of vapor and α_{v} denotes its volume fraction. μ_{l} is the viscosity of water and μ_{v} is the viscosity of vapor.

2.2 Turbulence Model

Turbulent flow is the irregular, multi-scale, three-dimensional, and non-constant flow. SST k-ω turbulence model [11], which combined advantages of k-ε models and standard k-ω model, was employed to solve the turbulent flow. The equations are shown below.

$$\rho_{\mathrm{m}}\frac{\partial k}{\partial t}+\rho_{\mathrm{m}}u_j\frac{\partial k}{\partial x_j}=G_k-\rho_{\mathrm{m}}\beta_*\omega k+\frac{\partial}{\partial x_j}\left[\left(\mu+\frac{\mu_{\mathrm{t}}}{\sigma_k}\right)\frac{\partial k}{\partial x_j}\right] \tag{6}$$

$$\rho_{\mathrm{m}}\frac{\partial \omega}{\partial t}+\rho_{\mathrm{m}}u_j\frac{\partial \omega}{\partial x_j}=\alpha G_\omega-\rho_{\mathrm{m}}\beta\omega^2+\frac{\partial}{\partial x_j}\left[\left(\mu+\frac{\mu_{\mathrm{t}}}{\sigma_\omega}\right)\frac{\partial \omega}{\partial x_j}\right]$$
$$+2\rho_{\mathrm{m}}(1-F_B)\frac{1}{\sigma_{\omega_{\mathrm{out}}}\omega}\frac{\partial k}{\partial x_j}\frac{\partial \omega}{\partial x_j} \tag{7}$$

where k is turbulent kinetic energy and G_k is corresponding generating term. ω is specific dissipation rate and G_ω is corresponding generating term. F_{B} is the blending function. μ_{t} is turbulent viscosity. α, β, σ_k, and σ_ω are empirical constants. For β_*, the value is 0.09. The value of $\sigma_{\omega\mathrm{out}}$ is 1.176.

Similar with the correction of turbulent viscosity in the k-ε model [12], turbulent viscosity in SST k-ω model was corrected as well. The correction function is shown in Fig. 1. Purpose to reduce the turbulent viscosity in cavitation region was achieved. Therefore, cavitation bubble shedding process under adverse pressure gradient condition was captured better. The value of n was 10. Equations are as follows.

$$\mu_t=f(\rho)\frac{k}{\omega} \tag{8}$$

$$f(\rho)=\rho_v+\frac{(\rho_m-\rho_v)^n}{(\rho_l-\rho_v)^{n-1}}\quad(n\geq 1) \tag{9}$$

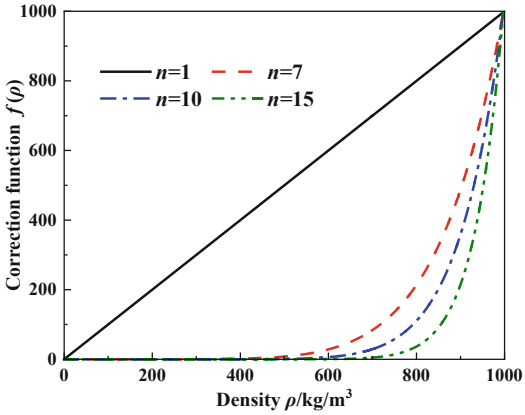

Fig. 1. Correction function of the density.

2.3 Cavitation Model

Zwart-Gerber-Belamri cavitation model [13] is the improvement of Kubota model [14], which could better describe unsteady flow characteristics of cavitation flow. The model assumes that cavitation bubble radius is the constant and their interphase mass transfer rate per unit volume is estimated by the number density of cavitation bubbles and mass change rate of individual bubble. Equations for evaporation and condensation source terms are shown below.

$$m_e = F_{vap}\frac{3\alpha_{nuc}(1-\alpha_v)\rho_v}{r_b}\sqrt{\frac{2}{3}\frac{p_v - p}{\rho_l}} \quad p < p_v \tag{10}$$

$$m_c = F_{cond}\frac{3\alpha_v\rho_v}{r_b}\sqrt{\frac{2}{3}\frac{p - p_v}{\rho_l}} \quad p > p_v \tag{11}$$

where r_b is cavitation bubble radius and the value is 1×10^{-6} m. α_{nuc} is the volume fraction of cavitation nuclei; p_v is saturated vapor pressure, taken as 3169 Pa in the numerical simulation process. F_{vap} is evaporation coefficient with a value of 50 and F_{cond} is the condensation coefficient with a value of 0.01 [12].

3 Numerical Simulation Setup

3.1 Physical Model

Physical models of general hydrofoil and the hydrofoil with rectangular structure on the surface are shown in Fig. 2. Angle of attack is $\alpha = 8°$, chord length is $C = 0.1$ m, and spanwise width is 4 mm. Front of the rectangular structure is located at the position of 55% chord length of the hydrofoil; its height is $b = 1.7$ mm and the length is $l = 5.5$ mm.

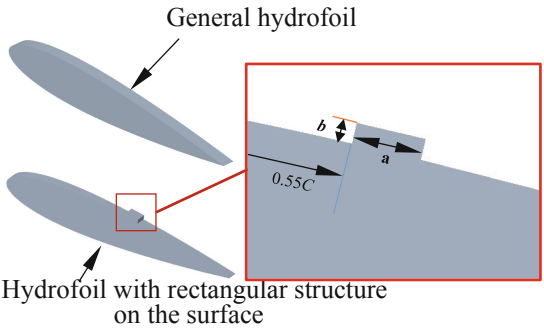

Fig. 2. Physical model.

3.2 Mesh Generation

Mesh discretization was performed by the commercial software of ANSYS-ICEM. To better fit the mesh with the computational domain boundary, unstructured tetrahedral meshes were employed. Also, meshes near the wall were refined. Mesh height of the first layer was 0.001 and the growth rate was 1.2. Number of mesh level with boundary layer thickness of 3 was 15. Total mesh number for general hydrofoil was 613314. For the hydrofoil with rectangular structure on the surface, it was 773167. They are shown in Fig. 3.

3.3 Boundary Conditions

Computational domain and boundary conditions are shown in Fig. 4. Distance between leading edge with inlet was $2.5C$. For distance between trailing edge with outlet, it was $7.5C$. Distance between the hydrofoil center with upper or lower wall was $1C$. Velocity was set as inlet, taken as 10 m/s. Cavitation number was $\sigma = 0.8$. Pressure was given at outlet and the value calculated was 43049 Pa. Time step was $\Delta t = 5 \times 10^{-5}$ s and the total time was 0.6 s.

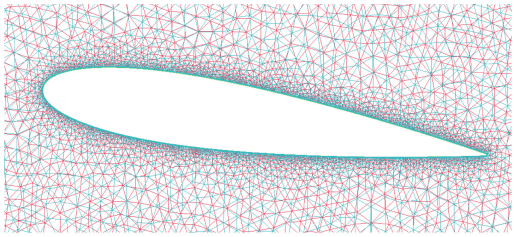

(a) General hydrofoil

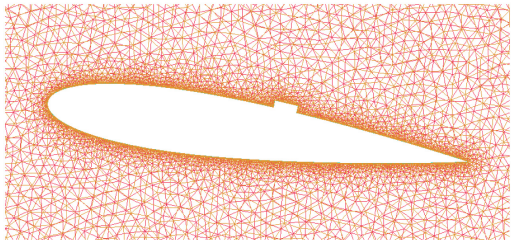

(b) Hydrofoil with rectangular structure on the surface

Fig. 3. Meshes of the computational domain.

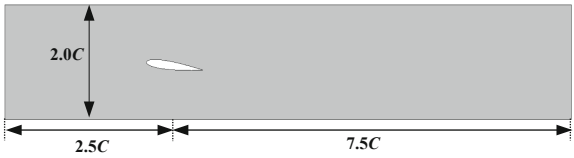

Fig. 4. Computational domain and boundary conditions.

4 Results and Discussion

4.1 Variations of Hydrodynamic Performances

Equations for lift and drag coefficients and lift-drag ratio are shown below:

$$C_L = \frac{L}{0.5\rho_l V_\infty^2 A} \tag{12}$$

$$C_D = \frac{D}{0.5\rho_l V_\infty^2 A} \tag{13}$$

$$K = \frac{C_L}{C_D} \tag{14}$$

where C_L and C_D are lift coefficient and drag coefficient, respectively; L and D are lift and drag, which act on the hydrofoil. K is lift-drag ratio. A is projected area in the plane where chord length is located.

Time domain variations of lift-drag ratio are shown in Fig. 5. The average lift-drag ratio for the hydrofoil with rectangular structure on the surface was 3.44, which was 15.98% greater than that of general hydrofoil. It indicated that hydrodynamic performances of the hydrofoil with rectangular structure on the surface were improved. Flow around this hydrofoil was more stable than that of general hydrofoil.

4.2 Evolution of Cavitation Bubbles and Vortices

Figures 6, 7, 8, 9 and 10 show evolution process of cavitation bubbles and distributions of streamlines at different moments for general hydrofoil and the hydrofoil with rectangular structure on the surface.

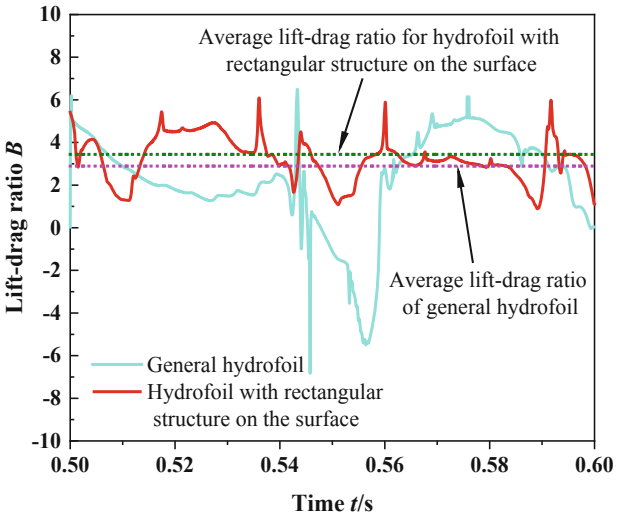

Fig. 5. Time domain analysis of lift-drag ratio.

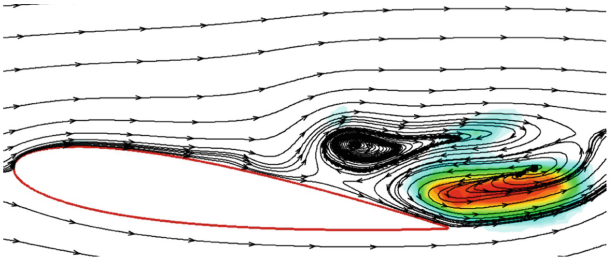

(a) General hydrofoil

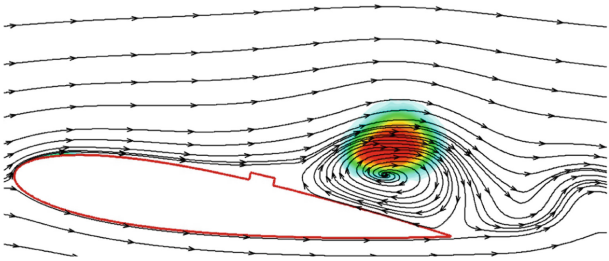

(b) Hydrofoil with rectangular structure on the surface

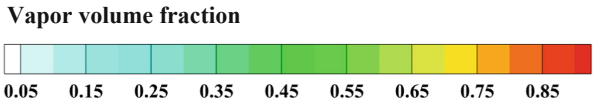

Fig. 6. Variations of cavitation bubbles and streamlines at $t = t_0$.

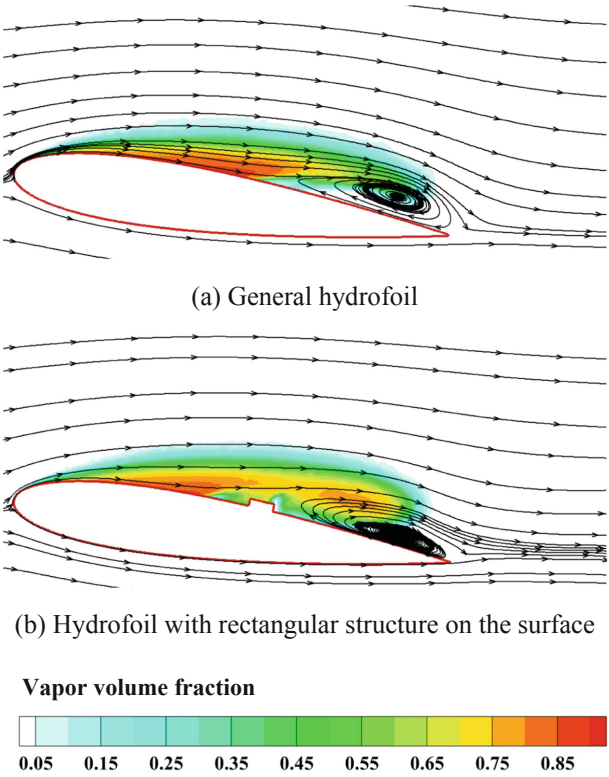

Fig. 7. Variations of cavitation bubbles and streamlines at $t = t_0 + 2/8T$.

T denoted one cycle and the value was 0.05 s. When $t = t_0$, both hydrofoils formed tiny attached cavitation bubbles at leading edge. For general hydrofoil, one long and narrow bubble existed at trailing edge; the volume was significantly larger than that of the hydrofoil with rectangular structure on the surface. Two interacting vortices around the suction surface of general hydrofoil existed and the distribution scope was particularly large. However, only one vortex appeared on the suction surface of the hydrofoil with rectangular structure on the surface; the scope was small. Both for these two hydrofoils, attached bubbles became the maximum ones at $t = t_0 + 2/8T$. For general hydrofoil, the bubble length was about $0.95C$; at trailing edge, shape of cavitation bubbles which were off the hydrofoil surface was concave. For the hydrofoil with rectangular structure on the surface, the bubble length was about $0.9C$ and shape of bubbles at trailing edge was elliptical. Distributions of vortices were almost identical. Under $t = t_0 + 4/8T$, attached bubbles were off suction surface and moved towards the downstream. Influenced by the

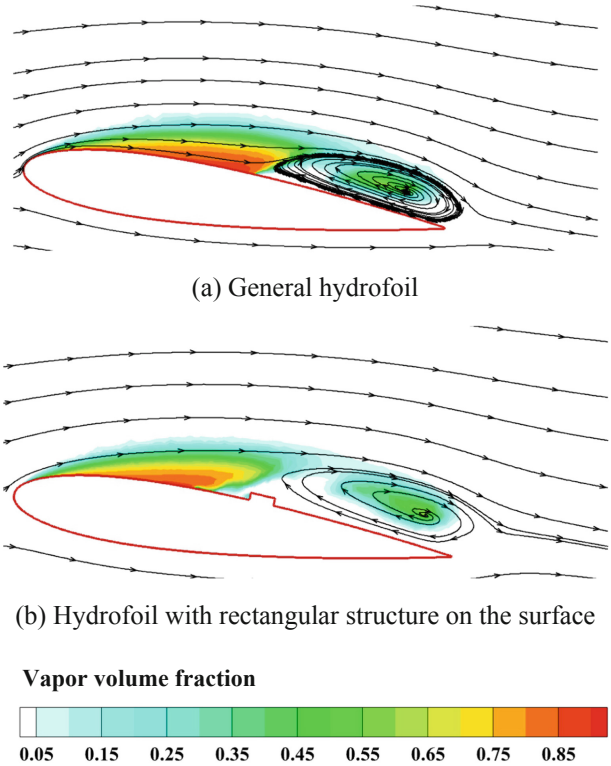

Fig. 8. Variations of cavitation bubbles and streamlines at $t = t_0 + 4/8T$.

rectangular structure, the vapor volume fraction was significantly lower than that of the general hydrofoil. The distribution scope of vortices was relatively smaller than that of the general hydrofoil. When $t = t_0 + 6/8T$, there were two cavitation bubbles on suction surface of the general hydrofoil; one was particularly large and the other one was minute. For the hydrofoil with rectangular structure on the surface, only one small cavitation bubble appeared. Differences of the distribution scope of vortices of these two hydrofoils were the largest one during the whole cycle. At $t = t_0 + 8/8T$, cavitation bubbles around the general hydrofoil were larger than those of the hydrofoil with rectangular structure on the surface. For vortices, variations of the distribution scope were almost identical.

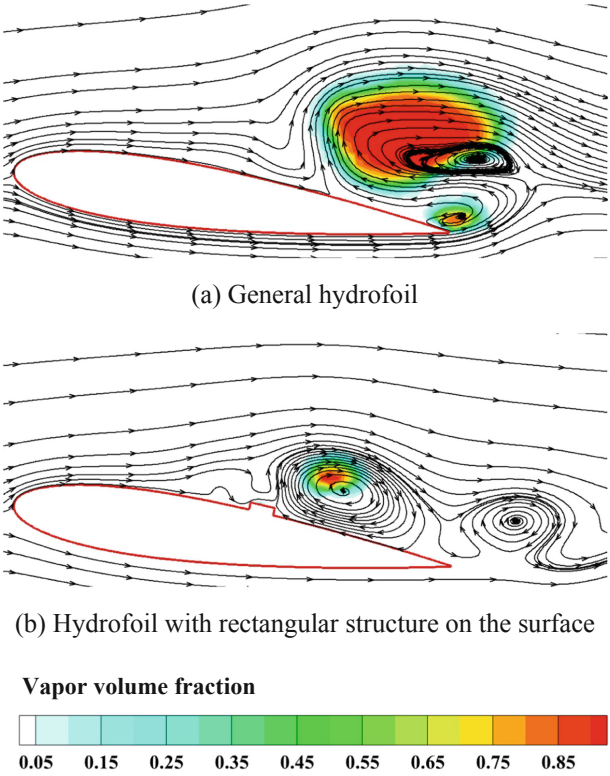

Fig. 9. Variations of cavitation bubbles and streamlines at $t = t_0 + 6/8T$.

For the whole process, effects of rectangular structure on the suction surface on the suppression of cavitation bubble evolution were remarkable. The influences of vortices on flow fields were weaker than those of the general hydrofoil. Therefore, cavitation flow field around the hydrofoil with rectangular structure on the surface was more stable.

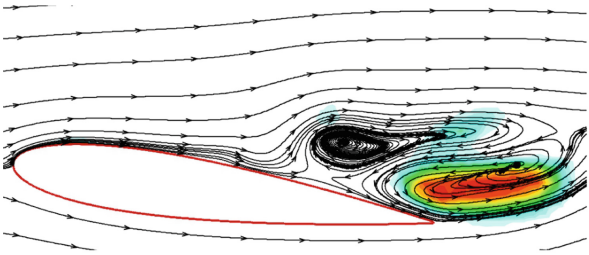

(a) General hydrofoil

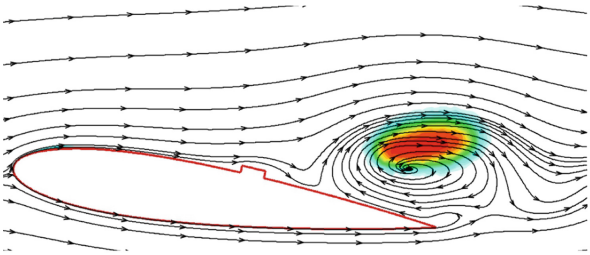

(b) Hydrofoil with rectangular structure on the surface

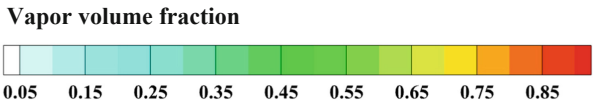

Fig. 10. Variations of cavitation bubbles and streamlines at $t = t_0 + 8/8T$.

5 Conclusions

Numerical simulations on cavitation flow around general hydrofoil and the hydrofoil with rectangular structure on the surface were performed to investigate effects of rectangular structure on the inhibition of cavitation bubble periodic evolution process. Variations of lift-drag ratio and evolution of cavitation bubbles and vortices were discussed. Main conclusions were as follows.

(1) Average lift-drag ratio of the hydrofoil with rectangular structure on the surface was greater than that of the general hydrofoil. Hydrodynamic performance was improved.
(2) For the hydrofoil with rectangular structure on the surface, cavitation bubble evolution degree in one cycle was weaker than that of general hydrofoil and the distribution scopes of streamlines were smaller than that of general hydrofoil. Flow field became more stable.

Acknowledgments. The investigation was financially supported by National Natural Science Foundation of China (Grant No. 52169018).

References

1. Ghadimi, A., Ghassemi, H.: Comparative assessment of hydrodynamic performance of two-dimensional Naca0012 and Naca6612 hydrofoils under different cavitation and non-cavitation conditions. Int. J. Hydromechatronics **3**(4), 349–367 (2020). https://doi.org/10.1504/IJHM.2020.112161
2. Koukouvinis, F., Gavaises, M.: Cavitation and Bubble Dynamics: Fundamentals and Applications. Academic Press (2021)
3. Kang, C., Liu, H.X., Song, L.B., Zhang, S.: Cavitation Erosion. Science Press (2020)
4. Wang, Y.Y., Zhao, W.G., Han, X.D., Fan, P.J., Liu, Z.L., Hu, J.Q.: Investigation on effects of bionic special configuration on hydrofoil surface on cavitation suppression. J. Xi'an Jiaotong Univ. https://doi.org/10.7652/xjtuxb202209000
5. Kawanami, Y., Kato, H., Yamaguchi, H., Tanimura, M., Tagaya, Y.: Mechanism and control of cloud cavitation. J. Fluids Eng. **119**(4), 788–794 (1997). https://doi.org/10.1115/1.2819499
6. Jin, W.: Cavitation generation and inhibition. II. Invisible tail wing of cloud cavitation and non-cavitation control mechanism. AIP Adv. **11**(11), 115216 (2021). https://doi.org/10.1063/5.0058785
7. Zhang, L.-X., Chen, M., Deng, J., Shao, X.-M.: Experimental and numerical studies on the cavitation over flat hydrofoils with and without obstacle. J. Hydrodyn. **31**(4), 708–716 (2019). https://doi.org/10.1007/s42241-019-0057-6
8. Liu, C., Yan, Q.D., Wood, H.G.: Numerical investigation of passive cavitation control using a slot on a three-dimensional hydrofoil. Int. J. Numer. Meth. Heat Fluid Flow **30**(7), 3585–3605 (2020). https://doi.org/10.1108/HFF-05-2019-0395
9. Shi, Z.H., Xie, Z.S., Shi, W.D., Zhang, Q.H., Tan, L.W.: Numerical investigation on cavitation suppression of microchannel over a NACA0012 hydrofoil. Shock. Vib. **2021**(6), 6641839 (2021). https://doi.org/10.1155/2021/6641839
10. Yeoh, G.H., Tu, J.: Computational Techniques for Multi-Phase Flows. Butterworth-Heinemann (2010)
11. Menter, F.R.: Two-equation eddy-viscosity turbulence models for engineering applications. AIAA J. **32**(8), 1598–1605 (1994). https://doi.org/10.2514/3.12149
12. Coutier-Delgosha, O., Stutz, B., Vabre, A., Legoupil, S.: Analysis of cavitating flow structure by experimental and numerical investigations. J. Fluid Mech. **578**, 171–222 (2007). https://doi.org/10.1017/S0022112007004934
13. Zwart, P.J., Gerber, A.G., Belamri, T.: A two-phaseflow model for predicting cavitation dynamics. In: Proceedings of ICMF 2004 International Conference on Multiphase Flow, Yokohama, Japan (2004)
14. Kubota, A., Kato, H., Yamaguchi, H.: AA new numerical simulation method of cavitating flow caused by large-scale vortices. Theoret. Appl. Mech. **36**, 93–100 (1998)